JGR Atmospheres

RESEARCH ARTICLE
10.1029/2020JD033630

Precipitation Characteristics and Future Changes Over the Southern Slope of Tibetan Plateau Simulated by a High-Resolution Global Nonhydrostatic Model

Ying Na[1,2], Riyu Lu[2,3], Qiang Fu[4], and Chihiro Kodama[5]

[1]Beijing Regional Climate Center, Beijing, China, [2]State Key Laboratory of Numerical Modeling for Atmospheric Sciences and Geophysical Fluid Dynamics, Institute of Atmospheric Physics, Chinese Academy of Sciences, Beijing, China, [3]College of Earth and Planetary Sciences, University of the Chinese Academy of Sciences, Beijing, China, [4]Department of Atmospheric Sciences, University of Washington, Seattle, WA, USA, [5]Japan Agency for Marine-Earth Science and Technology, Yokohama, Japan

Abstract Current climate model resolution cannot accurately describe the complex topography over the Tibetan Plateau, which limits our understanding of past and future precipitation over this region. This study investigates the daily precipitation characteristics and its future changes over the Tibetan Plateau, especially for the southern slope of Tibetan Plateau (SSTP), by 14-km Nonhydrostatic ICosahedral Atmospheric Model (NICAM) with explicitly calculated convection for historical and future 30-years period. By comparing with the satellite Global Precipitation Measurement (GPM), NICAM well reproduces the historical precipitation spatial pattern, seasonal cycle, and the extreme precipitation belt over SSTP, but overestimates precipitation amount by ~35%. It is found that heavy precipitation probability decreases as elevation becomes higher while the light precipitation generally shows the opposite. For the precipitation changes during June to September from 1979–2008 to 2075–2104, NICAM predicts that mean precipitation will decrease over low-level SSTP but increase over high-level SSTP. Nonprecipitation and heavy precipitation probability will increase while light precipitation probability will decrease in the future over SSTP. The extreme precipitation probability and intensity will increase ~50%/°C and ~8%/°C over SSTP, and this increase is more obvious as elevation becomes higher. The robust increase of extreme precipitation along the SSTP topography is unique and has not been identified by the climate model simulations before. The strong meridional gradient of specific humidity over SSTP is found to be further enhanced under global warming, and this gradient enhancement is suggested to be responsible for the increase in the extreme precipitation over SSTP.

Key Points:

- NICAM well reproduces precipitation spatial pattern, seasonal cycle, and extreme precipitation belt over SSTP as compared with observations
- Future mean precipitation over SSTP during the summer will decrease over lower SSTP but increase over higher SSTP from NICAM simulation
- The projected extreme precipitation will increase along the SSTP topography, especially over higher SSTP, at the end of the 21st century

Supporting Information:

- Supporting Information S1

Correspondence to:

R. Lu,
lr@mail.iap.ac.cn

Citation:

Na, Y., Lu, R., Fu, Q., & Kodama, C. (2021). Precipitation characteristics and future changes over the southern slope of Tibetan Plateau simulated by a high-resolution global nonhydrostatic model. *Journal of Geophysical Research: Atmospheres*, *126*, e2020JD033630. https://doi.org/10.1029/2020JD033630

Received 3 AUG 2020
Accepted 24 DEC 2020

1. Introduction

The Tibetan Plateau is the highest and most extensive highland in the world and is considered as the Asian water tower by hosting the headwaters of surrounding regions (Lin et al., 2018; Su et al., 2016; Xu et al., 2008). South Asian summer monsoon and orographic lifting process result in abundant precipitation, especially along south-facing slopes of the Tibetan Plateau (Bhatt & Nakamura, 2005; Wu & Zhang 1998; Zhang et al., 2019). Precipitation over the Tibetan Plateau is critical to river runoff, glacier mass balance, and water supply to human society (Bibi et al., 2018; Dong et al., 2016; Yang et al. 2012; Yao et al., 2012). On the other hand, landslides over steep region triggered by extreme precipitation cause hundreds to thousands of fatalities each year (Froude & Petley, 2018; Petley et al., 2007) and the landslide activity is expected to increase due to extreme precipitation changes under climate change (Kirschbaum et al., 2020). Therefore, the study of precipitation over southern slope of Tibetan Plateau (SSTP) and its future prediction has significant societal implications.

Characteristics of precipitation over SSTP have been investigated by many previous studies, including precipitation spatial distribution, temporal variability, and precipitation mechanism. The uplifting of topography was shown to have an important effect on precipitation (Fu et al., 2017; Liu & Dong, 2013; Zhang et al., 2015) and therefore the precipitation over SSTP exhibits a zonal distribution along the topography of valley and ridge (Anders et al., 2006; Bookhagen & Burbank, 2006; Fu et al., 2017; Zhang et al., 2018a). Precipitation also presents an increasing tendency from flat plain to lower SSTP below ~2.5 km but a decreasing tendency as elevation increase above ~2.5 km (Fu et al., 2017; Saler-

no et al., 2015; Yang et al., 2018). Some studies show that there are two remarkable rainfall peaks at ~0.9 and ~2.1 km (e.g., Bookhagen & Burbank, 2006; Shrestha et al., 2012). For temporal variability, most precipitation over SSTP concentrates on boreal summer (Bookhagen & Burbank, 2010; Palazzi et al., 2015; Shrestha et al., 2012) and presents a strong diurnal cycle (Chen, 2020; Hirose & Kenji, 2005; Liu et al., 2009). The sucking and pumping effects induced by surface sensible heating lead to climbing airflow and moisture convergence over southern Tibetan Plateau, which is one of the primary causes of local precipitation formation (Duan & Wu, 2005; Wu et al., 2007).

The Tibetan Plateau is one of the most sensitive regions to global climate change (Kuang & Jiao, 2016; Liu & Chen, 2000; Liu et al., 2009; Xu et al., 2008). Salerno et al. (2015) show a substantial rain weakening (−9.3 mm/year) and temperature increasing (0.044 °C/year) during the monsoon season over SSTP by analyzing the station observations during 1994–2013, which may lead to the glacier shrinkage in the Himalayas. Yao et al. (2012) and Lei et al. (2014) also show that precipitation changes accompanied by different atmospheric circulation patterns are probably driving lakes and glaciers changes over Tibetan Plateau for the past several decades. For future possible precipitation change under global warming, climate models predict more precipitation and intensive precipitation extremes over most of the Tibetan Plateau (Ali et al., 2015; Palazzi et al., 2015; Panday et al., 2015; Su et al., 2013; Wu et al., 2017). However, current climate models' spatial resolutions are too coarse to resolve the steep topography and associated small-scale processes, and thus they have limitation to investigate the topographic convection and the elevation-dependence of meteorological variables. Furthermore most climate models are proved to have wet bias over the Himalayan Mountains and Tibetan Plateau (Gao et al., 2011; Mehran et al., 2014; Mueller & Seneviratne, 2014; Su et al., 2013; Yu et al., 2015), which may be caused by the excess of water vapor transport toward the Tibetan Plateau (Lin et al., 2018) or higher intensity of intermittent events (Karki et al., 2017). Due to the limitation of climate models' resolution, few studies focus on the future precipitation change over steep slope region of south Tibetan Plateau which is the main focus of this study.

Finer model resolution can improve the precipitation simulation over complex terrain (e.g., Giorgi et al., 2016; Leung & Qian, 2003; Li et al., 2020; Mahoney et al., 2013; Torma et al., 2015), in particular for the magnitudes of daytime convective precipitation, at higher elevations (Collier & Immerzeel, 2015), and for the peak timings of diurnal precipitation cycle (Karki et al., 2017). Lin et al. (2018) indicates that higher-resolution simulations reduce the wet bias over Tibetan Plateau by producing more precipitation over the southern Himalayan slopes and weaker water vapor transport toward the Tibetan Plateau. Zhang et al. (2019) suggests that finer resolution model can better reproduce the spatial patterns and seasonal mean of precipitation and evaporation over the Tibetan Plateau. Improved parameterizations along with finer resolutions can also favor better simulations of the probability density distributions of precipitation. Lin et al. (2019) shows that climate models with higher horizontal resolution and upgraded physical parameterizations better simulate the probability density distributions of daily precipitation over Tibet. Bao and Li (2020) finds that a climate model (FGOALS-f3-L) with Resolving Convective Precipitation scheme more accurately reproduces the probability distribution of daily precipitation over the Tibetan Plateau in comparison with conventional convective parameterization. However, most of previous high-resolution simulations over the Tibetan Plateau just perform for a short period and few of them focus on future projection. Here, we investigate the precipitation and its future changes over the Tibetan Plateau, especially at the southern steep slope, by the Nonhydrostatic Icosahedral Atmospheric Model (NICAM), a global nonhydrostatic model with explicit convection calculations, for both historical (30 years) and future (30 years) periods.

This paper is organized as follows. Section 2 describes the data and methods. Section 3 shows the historical precipitation characteristics from satellite observation and evaluates the precipitation simulation from NICAM over the Tibetan Plateau. Section 4 presents the future prediction of precipitation and associated circulation at the end of 21st century from NICAM. Section 5 gives the conclusions and discussions.

2. Data and Methods

2.1. Observational and Model Data

Global Precipitation Measurement (GPM) is an international satellite mission that provide advanced observations of rain and snow worldwide. GPM Core Observatory (GPM-CO) was launched in 2014, including a dual-frequency precipitation radar (DPR) capable of providing information on precipitation vertical distributions, and a multifrequency passive-microwave imaging radiometer (GPM Microwave Imager, GMI) capable of sensing the total precipitation. GPM-CO make it possible to detect rain rates from 0.2 to 110.0 mm/h as well as moderate to intense snow events. GPM-CO serves as a reference for unifying the data from multiple satellites to provide next-generation precipitation products. Integrated Multisatellite Retrievals for GPM (IMERG) algorithm (including GPM-CO, TRMM, etc.), combining data from all passive-microwave instruments in the GPM mission, produces precipitation datasets with high temporal (up to 0.5 h) and spatial (up to 0.1°) resolutions over the entire globe (Hou et al., 2014; Huffman et al., 2015; Skofronick-Jackson et al., 2017). GPM IMERG could capture the spatial patterns of precipitation and precipitation probability density functions corresponding to ground gauge data (Lu & Yong, 2018), and generally performs better than TRMM (Tropical Rainfall Measuring Mission) (Zhang et al., 2018b). Note that TRMM itself cannot detect light precipitation (i.e., <0.5 mm/h) and snow events, which may be limited in application on high-elevation areas (Tian & Peters-Lidard, 2010). Precipitation characteristics over the southern slope of Tibetan Plateau were investigated by using GPM observations (Gao et al., 2019; Zhang et al., 2018a). In this study, we use GPM IMERG V06B Level3 daily data with 0.1° resolution from 2001 to 2008 to evaluate model precipitation simulation. The data can be accessed from https://gpm1.gesdisc.eosdis.nasa.gov/data/GPM_L3/GPM_3IMERGDF.06/. The GPM data with 0.1° resolution are regridded to the horizontal resolution of model (0.14°) for the comparison by using bilinear interpolation from the Earth System Modeling Framework (ESMF, https://www.earthsystemcog.org/projects/regridweightgen/).

The Non-hydrostatic Icosahedral Atmospheric Model (NICAM), a global atmospheric model, is designed on a nonhydrostatic equation system and a quasi-uniform grid mesh structure (Satoh et al., 2008, 2014; Tomita & Satoh, 2004). We use the climate simulation from the NICAM.12 version for both historical and future periods (Kodama et al., 2015; Satoh et al., 2015). The horizontal resolution is 14 km and there are 38 vertical levels extending to 40 km above the sea level. Water vapor, liquid cloud, ice cloud, rain, snow, and graupel were predicted with the NICAM single-moment water 6-cloud microphysics scheme (NSW6) (Tomita, 2008). Without a cumulus convection parameterization, the NICAM with a 14-km grid is capable to resolve similar gross features of convective circulation as cloud resolving model with much higher resolution (Kajikawa et al., 2016; Miyamoto et al., 2013). The temporally evolving monthly sea surface temperatures (SST) and sea ice from observations were used for historical simulation. For future simulation, the SST and sea ice were estimated based on CMIP3 model ensemble mean with a correction that eliminates the present-day climate simulation bias (Mizuta et al., 2008; Satoh et al., 2015). The corresponding annual mean concentrations of CO_2, N_2O, CH_4, CFC_{11}, and CFC_{12} were set uniformly globally (Hansen & Sato, 2004) and without considering of aerosols and solar cycles. NICAM can well simulate the spatiotemporal variations of convective clouds over Tibetan Plateau (Sato et al., 2007, 2008), and diurnal precipitation cycle and nocturnal precipitation over southern slope of the Tibetan Plateau (Dirmeyer et al., 2011). It has been used to investigate the response of global precipitation and monsoon precipitation to climate change in the future (e.g., Na et al., 2020; Takahashi et al., 2020). Herein, we focus on the Tibetan Plateau by using the NICAM AMIP-type simulation for the historical period from 1979 to 2008 and future period from 2075 to 2104 under A1B scenario. The global-mean surface temperature change is 2.67 °C from the historical to future periods considered. The hourly precipitation data are converted to daily-mean data with a 14-km horizontal resolution. Wind and specific humidity data are used with 1° resolution. The terms and guideline of NICAM data can be accessed from http://nicam.jp/hiki/?Research+Collaborations.

Figure 1 shows the topography of the Tibetan Plateau based on the NOAA ETOPO1 data with a 1 arc-min resolution (https://ngdc.noaa.gov/mgg/global/global.html) as compared with the topography used in NICAM with 14-km resolution. Although the topography in NICAM is smoothed for the stable numerical integration and loses many detailed descriptions of elevation higher than 5,000 m, it can capture

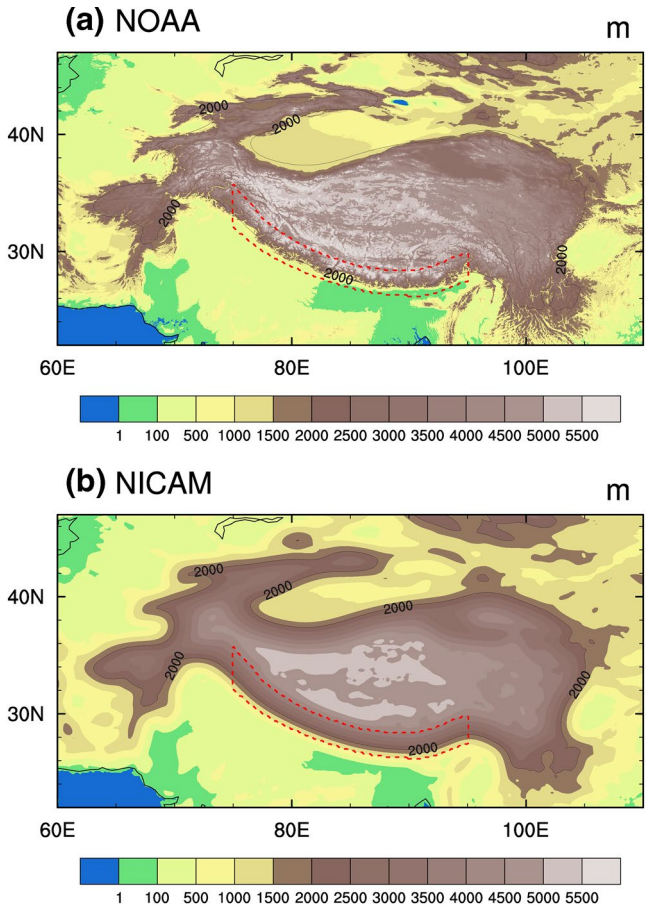

Figure 1. Topography of the Tibetan Plateau from (a) NOAA with 1 arc-min resolution and (b) NICAM with 14-km resolution, unit: m. The black line is 2,000-m contour line in NICAM. The red dash line shows the area where elevation falls in 1,000–4,000 m between 75°E and 95°E in NICAM, which is defined as southern slope of Tibetan Plateau (SSTP) in this study. NICAM, Nonhydrostatic ICosahedral Atmospheric Model.

the major relief features including the 2,000-m contour of the Tibetan Plateau. The topographic structure of the Tibetan Plateau in NICAM is finer than most current climate models.

2.2. Analysis Methods

We define the area where elevation falls in 1,000–4,000 m between 26°N and 36°N, 75°E–95°E in NICAM as the southern slope of Tibetan Plateau (SSTP) (Figure 1), following Fu et al. (2017) and Zhang et al. (2018) based on the steep topography (Figure 1) and heavy precipitation region (Figure 2). The part of SSTP where elevation falls in 1–2, 2–3, and 3–4 km is defined as low-level, middle-level, and high-level SSTP, respectively. Since the main rainy season over SSTP typically lasts from June to September associated with India summer monsoon (Palazzi et al., 2015; Zhang et al., 2018a), our studies focus on the boreal summer from June to September.

We examine the precipitation frequency in terms of daily precipitation intensities (mm/d) starting from 0.1 mm/d. Here, nonprecipitating day is defined when daily precipitation intensity is smaller than 0.1 mm/d (Dai et al., 2018). Probability density function (PDF) is derived over each grid cell and then averaged over specific area. The percentage change for future scenario relative to historical period is scaled by the global-mean temperature change of 2.67 °C.

The approach for quantifying the precipitation change scaled by local percentiles is based on Fischer and Knutti (2015, 2016). Daily precipitation percentiles are first derived by considering all days during June to September in historical and future periods, respectively, over each grid cell where each percentile corresponds to an absolute daily precipitation intensity. For example, 95% corresponds to x mm/d and y mm/d in historical and future period, respectively. The number of days with a daily precipitation intensity lager than x (y) mm/d over this grid cell is 183 days in historical (future) period. The percentage change of precipitation intensity scaled by temperature change for a given percentile is defined as $(y - x)/x$ ◊100%/2.67 °C. Suppose that the future probability of precipitation intensity larger than x mm/d is m%. The percentage change of precipitation probability is (m%–5%)/5%◊100%/2.67 °C. We then derive the average over specific area.

3. Historical Precipitation From Observation and Model

Figure 2 shows the annual mean precipitation and summer-mean precipitation from GPM and NICAM and their difference over the Tibetan Plateau from 2001 to 2008. Precipitation decreases from southeast to northwest of the Tibetan Plateau. Precipitation over SSTP obviously stands out and there are two precipitation maxima at southeast of the Tibetan Plateau. NICAM can well simulate the precipitation distribution as observation. Annual mean precipitation over most of the Tibetan Plateau is <2 mm/d. The annul mean precipitation averaged over SSTP is 3.68 mm/d from GPM and 5.17 mm/d from NICAM (Figures 2a and 2c). Precipitation in the summer from June to September is much larger than annual mean, especially over SSTP. The maximum summer precipitation over SSTP is 19.8 (24.3) mm/d from GPM (NICAM) and the summer-mean precipitation averaged over SSTP is 7.73 (10.48) mm/d (Figures 2b and 2d). From the difference between NICAM and GPM, NICAM overestimates both annual and summer-mean precipitation over the whole Tibetan Plateau including SSTP (Figures 2e and 2f). NICAM shows similar bias as compared with gauge observation data (See Supplementary Figure S1).

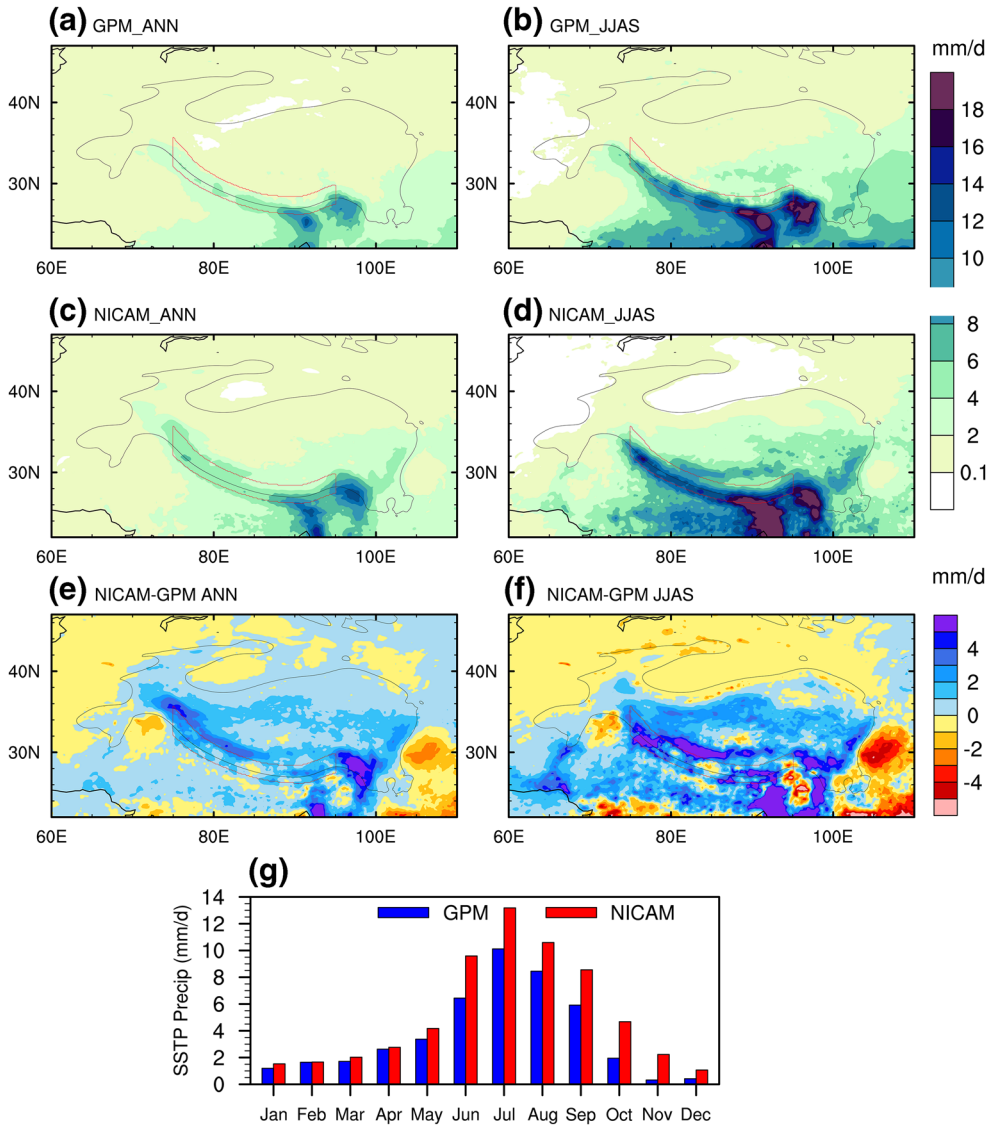

Figure 2. Precipitation (a and b) observed by GPM, (c and d) simulated by NICAM, and (e and f) difference between NICAM and GPM for (a, c, and e) annual mean and (b, d, and f) summer mean from June to September during 2001–2008, unit: mm/d. The black line is 2,000 m elevation contour and the red line shows SSTP area. (g) Monthly means of precipitation averaged over SSTP during 2001–2008 from GPM and NICAM, unit: mm/d. NICAM, Nonhydrostatic ICosahedral Atmospheric Model; GPM, Global Precipitation Measurement; SSTP, southern slope of Tibetan Plateau.

Wet bias over Tibetan Plateau in the NICAM is also seen in both CMIP5 and CMIP6 model simulations (e.g., Mehran et al., 2014; Mueller & Seneviratne, 2014; Su et al., 2013; Zhu & Yang, 2020). The average summer precipitation bias over Tibetan Plateau in NICAM is about 50%, while the bias in the CMIP5 (CMIP6) multimodel ensemble mean is about 80% (70%) (Su et al., 2013; Zhu & Yang, 2020) and these studies do not focus on the southern slope. Sato et al. (2007) suggested that the stronger upslope flow owing to the smoothed topography may lead to the stronger convection over SSTP in NICAM. The annual cycle of monthly precipitation averaged over SSTP is shown in Figure 2g. NICAM well captures the annual cycle observed by GPM, but overestimates the precipitation especially from June to November. In the following analysis, we focus on the precipitation over SSTP from June to September.

Figure 3a shows the precipitation probability density functions (PDFs) and nonprecipitation fractions from GPM and NICAM averaged over SSTP for June to September during 2001–2008. PDF denotes time

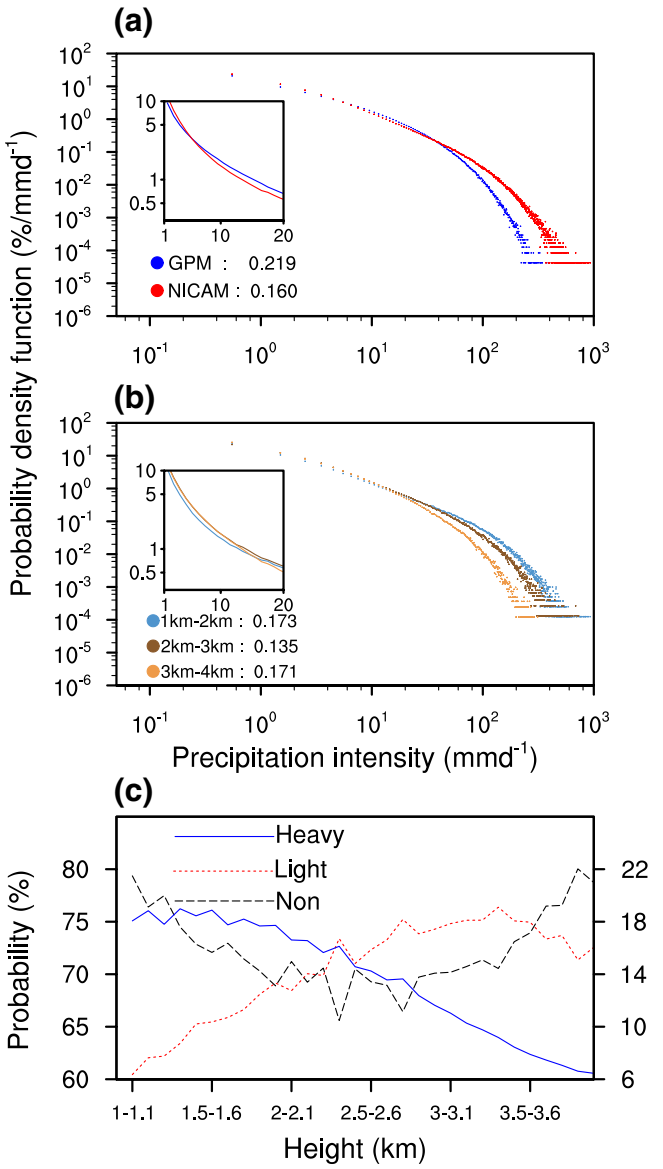

Figure 3. (a) Probability density function (PDF) of daily precipitation vs. precipitation intensity with a bin size of 1 mm/d averaged over SSTP for June to September during 2001–2008 from GPM and NICAM. (b) Same as (a), but for PDF averaged over low-level, middle-level, and high-level SSTP from NICAM. The small insert is a blowout for the precipitation intensity range between 1 and 20 mm/d. The nonprecipitation fractions (<0.1 mm/d) are also provided. (c) Probability of nonprecipitation (<0.1 mm/d) (right), light precipitation (0.1–20 mm/d) (left), and heavy precipitation (>20 mm/d) (right) averaged over bins of SSTP with a vertical bin size of 100 m vs. the corresponding topography height for June to September during 2001–2008 from NICAM. NICAM, Nonhydrostatic ICosahedral Atmospheric Model; GPM, Global Precipitation Measurement; SSTP, southern slope of Tibetan Plateau.

frequency, i.e., larger PDF means there are more days in precipitation with specific intensity. Nonprecipitation fraction over SSTP observed by GPM is 0.219 which is higher than 0.160 from NICAM. NICAM generally underestimates light precipitation PDF but overestimates heavy precipitation with intensity larger than ~30 mm/d. The largest precipitation intensity observed by GPM is ~400 mm/d, while NICAM can simulate precipitation larger than 800 mm/d. The wet bias of mean precipitation over SSTP shown in Figure 2 may be caused by the overestimation of heavy precipitation in NICAM. Figure 3b gives the precipitation PDFs over low-level, middle-level, and high-level SSTP from NICAM. Figure 3c shows the probability of nonprecipitation (<0.1 mm/d), light precipitation (0.1–20 mm/d), and heavy precipitation (>20 mm/d) averaged over different altitudes of SSTP. Although the precipitation over the whole SSTP is abundant, the precipitation probability shows different distribution over different levels. The nonprecipitation fraction over middle-level SSTP is the smallest. The heavy precipitation probability decreases as elevation becomes higher while the light precipitation PDFs generally show the opposite.

Figure 4 shows the spatial distributions of probability (%) for (a) nonprecipitation (<0.1 mm/d), (b) drizzle precipitation (0.1–1 mm/d), (c) light precipitation (1–20 mm/d), (d) heavy precipitation (20–100 mm/d), and (e) extreme heavy precipitation (>100 mm/d) from NICAM for June to September during 2001–2008. The same but from GPM observations is shown in Figure S2. Drizzle, light, heavy, and extreme heavy precipitation contributes to 1% (1%), 26% (40%), 47% (52%), and 26% (7%) of the total precipitation over SSTP from NICAM (GPM), respectively. Nonprecipitation probability from NICAM over most north Tibetan Plateau is larger than 40–50% but is much lower over SSTP and near-by regions with a mean value of 16% over SSTP (Figure 4a). Compared with GPM, NICAM overestimates nonprecipitation probability over north Tibetan Plateau but underestimates it over south Tibetan Plateau including SSTP (Figure S3). The drizzle and light precipitation probability over SSTP are 21.2% and 49.6%, respectively, from NICAM (Figures 4b and 4c), which does not show a systematic bias over SSTP as compared with GPM. Figure 4d shows that the probability for heavy precipitation ranging from 20 to 100 mm/d is 11.6% over SSTP. NICAM overestimates heavy precipitation probability over high-level SSTP but underestimates it over low-level SSTP. The probability of precipitation larger than 100 mm/d is only 1.65% over SSTP (Figure 4e). The extreme heavy precipitation probability over SSTP from NICAM is higher than GPM. NICAM simulations in most areas over SSTP do not show significant differences from GPM observations for the probability of drizzle, light, and heavy precipitation, but exhibit significant differences for extreme heavy precipitation probability. This suggests that the NICAM wet bias over SSTP mainly comes from the overestimation of extreme heavy precipitation probability. Besides, over the surrounding regions of Tibetan Plateau, such as Tian Shan Mountains and Sichuan Basin, NICAM overestimates nonprecipitation probability but underestimates drizzle and light precipitation probability (Figure S3) and dry bias exhibits over these regions (Figure 2f). The effects of complex terrain on precipitation through, e.g., uplifting of westerly flow over Tian Shan Mountains and downdraft from eastern Tibetan Plateau over Sichuan Basin, are still difficult to be reliably simulated.

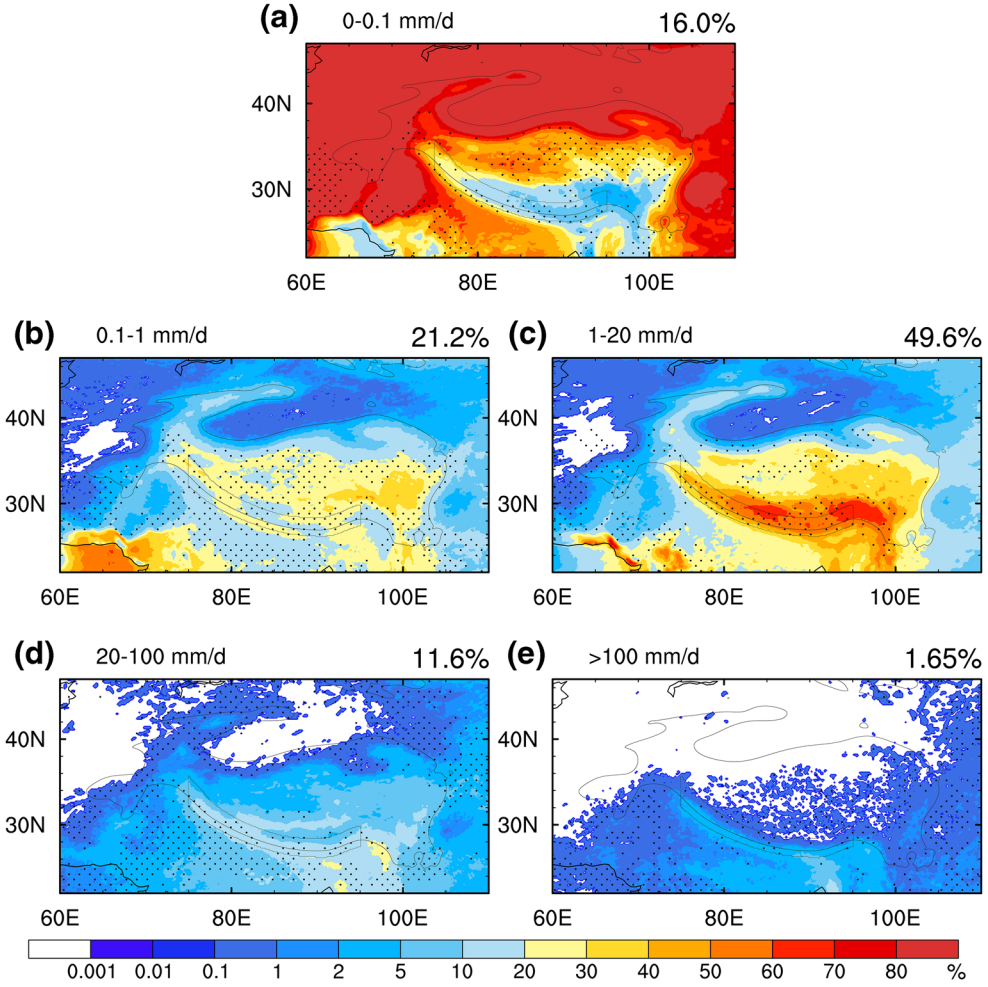

Figure 4. Spatial distributions of probability (%) for (a) nonprecipitation (<0.1 mm/d), (b) drizzle precipitation (0.1–1 mm/d), (c) light precipitation (1–20 mm/d), (d) heavy precipitation (20–100 mm/d), and (e) extreme heavy precipitation (>100 mm/d) from NICAM for June-September during 2001–2008. The dotted areas indicate that the difference between NICAM and GPM is statistically insignificant at the 95% level using the Mann Whitney test. The corresponding probability averaged over SSTP is also given. The black lines show 2000 m elevation and the surrounded SSTP area. NICAM, Nonhydrostatic ICosahedral Atmospheric Model; GPM, Global Precipitation Measurement; SSTP, southern slope of Tibetan Plateau.

4. Future Change Projections

4.1. Mean Precipitation and Precipitation Probability Changes

Figure 5a shows simulated summer precipitation changes in the future of 2075–2104 with respect to 1979–2008 over the Tibetan Plateau. For the entire Tibetan Plateau region, precipitation over the southeast area will decrease but increase over the middle-west area. The precipitation gradient from southeast to northwest will become weaker in the future. The precipitation change over most of the Tibetan Plateau is <1 mm/d. For the SSTP, low-level SSTP and lower surrounding area exhibit negative change but high-level SSTP exhibits positive change. This result differs from the CMIP5 multimodel mean with 2° resolution which shows the precipitation for June to September will increase uniformly over the whole Himalaya region at the end of 21st century under RCP 8.5 scenario (Palazzi et al., 2015). Figure 5b shows the precipitation for both historical and future periods averaged over every 100 m elevation area of the SSTP. The precipitation generally decreases with elevation, similar to the observation from TRMM satellite radar (Anders et al., 2006). Future precipitation will decrease over 1–2 km of SSTP but increase over 2–4 km of SSTP. The precipitation decrease with elevation will thus become weaker in the future. Coarse resolution climate models can hard-

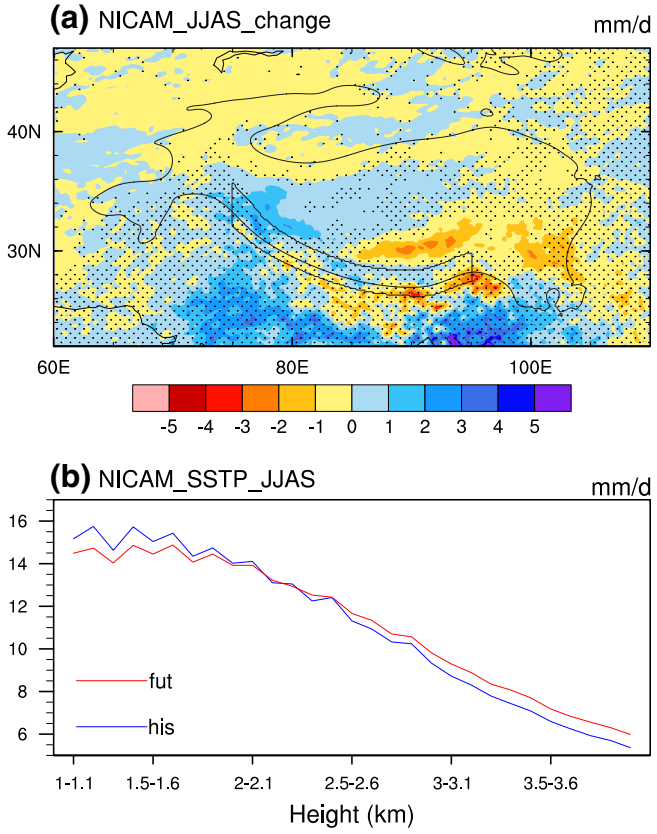

Figure 5. (a) Precipitation (mm/d) change in June to September for 2075–2104 vs. 1979–2008 from NICAM. The black lines show 2000-m contour line and SSTP area. The dotted area indicates the change is statistically significant at the 95% confidence level (Student's *t*-test). (b) Precipitation (mm/d) averaged over bins of SSTP with a vertical bin size of 100 m vs. the corresponding topography height for June to September during historical period 1979–2008 and future period 2075–2104. NICAM, Nonhydrostatic ICosahedral Atmospheric Model; SSTP, southern slope of Tibetan Plateau.

ly resolve the precipitation changes as detailed in Figure 5 (e.g., Palazzi et al., 2015; Wu et al., 2017).

Figure 6 shows the percentage change of nonprecipitation fractions and precipitation PDFs over the whole SSTP and low-level, middle-level, and high-level SSTP. The nonprecipitation fraction averaged over SSTP will increase 3.12% per degree global warming. The drizzle precipitation probability will increase and the light precipitation probability will decrease. For heavy precipitation larger than ~60 mm/d, the PDF is projected to increase greatly. The PDFs averaged over different levels of SSTP present different changing distributions. The increasing tendency of nonprecipitation probability decrease as elevation becomes higher. The future heavy precipitation probability will increase greater over high-level SSTP than over low-level SSTP.

Figure 7 presents the spatial distributions of future precipitation probability percentage changes relative to historical period for five precipitation ranges from NICAM. Most of the Tibetan Plateau exhibits an increase in nonprecipitation probability, especially for southeast Tibetan Plateau (Figure 7a) where the historical nonprecipitation probability is the smallest of Tibetan Plateau (Figure 4a), while part of west Tibetan Plateau exhibits a slight decrease. The drizzle precipitation probability will increase over SSTP and near-by regions but decrease over other parts (Figure 7b). Light precipitation probability will decrease over most areas including SSTP except part of west Tibetan Plateau (Figure 7c). Heavy precipitation probability for rain intensity between 20 and 100 mm/d shows an increase over west Tibetan Plateau but a decrease over southeast Tibetan Plateau and SSTP (Figure 7d). For extreme heavy precipitation larger than 100 mm/d, the probability will increase significantly over the SSTP and near-by regions with elevation above 2,000 m (Figure 7e). Note that the mixed pattern of both large increasing and decreasing trend over central Tibetan Plateau (Figure 7e) are caused by very few samples of extreme heavy precipitation days (Figure 4e), which make the future projections not statistically reliable. For precipitation over west Tibetan Plateau, near Karakoram Mountains (about 35°N, 77°E, higher than 8 km), where the elevation in NICAM uplifts higher than 5 km, both total precipitation probability and heavy precipitation probability will increase in the future. For precipitation over SSTP and surrounding slope area, especially 2–4 km area, the total precipitation probability will decrease while the extreme heavy precipitation probability will increase significantly.

4.2. Extreme Precipitation Changes

Precipitation intensity varies greatly over the Tibetan Plateau and extreme heavy precipitation probability presents an obvious increase in the future over SSTP. Here, we examine extreme precipitation changes scaled by local precipitation percentiles (see Section 2.2). Figure 8a shows the precipitation intensity (mm/d) corresponding to different percentiles (%) for June to September during historical period. For a given percentile larger than ~50%, precipitation intensity decreases with elevation which is consistent with a decrease of mean precipitation with elevation (Figure 5b). Precipitation intensity averaged over the whole SSTP shows similar distribution as middle-level SSTP. Future relative changes of precipitation intensity corresponding to different percentiles are shown in Figure 8b. Over low-level SSTP, about 93% of precipitation will become weaker in the future but the largest ~7% of precipitation will be stronger. Over the middle-level and high-level SSTP regions, the largest ~10% and ~15% of precipitation will be stronger, respectively. The increase in extreme precipitation intensity increases with percentiles and reaches to an extremum for the

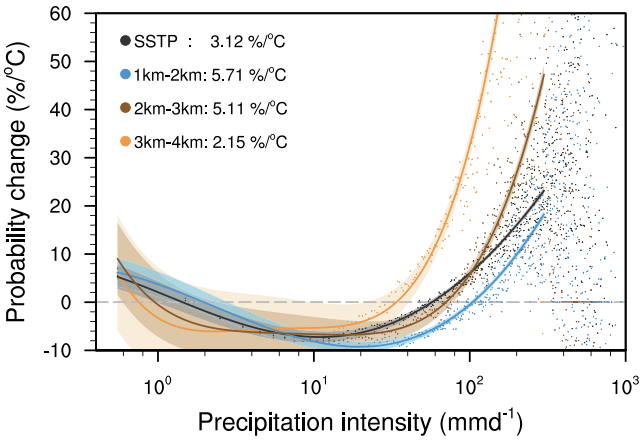

Figure 6. Percentage change (%/°C) of precipitation probability density functions (PDFs) in June to September during future period relative to historical period averaged over SSTP and portions of SSTP, scaled by global-mean temperature increase, from NICAM. The dots are the changes for precipitation intensities with an increment of 1 mm/d. The lines are polynomial fitting curves for precipitation intensity smaller than 300 mm/d and the shades are 95% confidence boundaries. The values are relative changes of nonprecipitation fractions (<0.1 mm/d) per degree global warming. NICAM, Nonhydrostatic ICosahedral Atmospheric Model; SSTP, southern slope of Tibetan Plateau.

precipitation percentile larger than 99%. Extreme precipitation intensity increases more over high-level SSTP than over low-level SSTP in the future. For extreme precipitation probability change shown in Figure 8c, it also increases over high-level SSTP more than over low-level SSTP. The relative change of extreme precipitation probability is larger than precipitation intensity. Stronger extreme precipitation will happen more frequently over SSTP, especially for high-level SSTP, in summer at the end of 21st century from NICAM simulation.

Figure 9 shows spatial distribution of precipitation intensity corresponding to 95%, 99%, 99.9% percentiles for historical summer (Figures 9a1–9c1), corresponding percentage changes in precipitation intensity (Figures 9a2–9c2) and precipitation probability (Figures 9a3–9c3) for the future period relative to historical period. The positive values in Figures 9a2–9c2 and 9a3–9c3 suggest that extreme precipitation will get stronger and more frequent in the future. The extreme precipitation intensity exhibits similar distribution to mean precipitation. Extreme precipitation intensity over southeast Tibetan Plateau is larger than over northwest Tibetan Plateau and precipitation over SSTP is much stronger (Figures 9a1–9c1). Future change of precipitation intensity over west Tibetan Plateau exhibits an increase for 95% (Figure 9a2), while the increase of precipitation intensity over SSTP is slightly stronger than other area for 99% and 99.9% (Figures 9b2and 9c2). The relative increase of precipitation probability is larger than intensity over SSTP (Figures 9a3–9c3), especially for 99% and 99.9%. Over SSTP, the distribution of the extreme precipitation probability increase aligns with the topography which is not simulated by previous climate models with coarser resolution. Extreme precipitation probability increases more over 2–4 km of SSTP than over 1–2 km of SSTP. Considering the heavy precipitation over SSTP and the steep terrain, the possible future intensified extreme precipitation under global warming is noteworthy since it may lead to more natural disasters such as flooding and landslides. In addition to SSTP, extreme precipitation exhibits a significant increase over west Tibetan Plateau which also locates at the windward slope for elevation higher than 5,000 m in NICAM.

Figure 10 is a global perspective of Figure 9b3. Extreme precipitation probability exhibits a significant increase over high-latitudes, north Pacific, tropical Pacific, South Asia, and surrounding regions, while it exhibits a decrease over parts of middle-latitudes. This changing tendency at the end of 21st century projected by NICAM agrees with previous climate models (e.g., Chen & Frauenfeld, 2014; Kharin et al., 2013). However, previous models cannot simulate the extreme precipitation change over SSTP. The relative increase of extreme precipitation probability over SSTP in the future is about 50%/°C, which is one of the regions in the north hemisphere with the largest increase and the distribution presents high consistency with topography. This possible change of extreme precipitation under global warming over SSTP is unique in the north hemisphere since extreme precipitation probability over other mountain regions, such as the Rockies and the Alps, does not exhibit such significant increasing tendency along topography.

4.3. Possible Mechanisms

Precipitation changes can be decomposed into contributions from atmospheric thermodynamics and dynamics (Chen et al., 2019; Pfahl et al., 2017). Figure 11 shows the spatial distribution of horizontal wind at 700 hPa and vertical velocity at 500 hPa from NICAM simulation for the historical period (Figures 11a and 11b) and their future changes (Figures 11c and 11d). Figures 11a and 11care based on the average of all days during June to September for 1979–2008 (3,660 days) and 2075–2104 (3,660 days). Figures 11b and 11d are the composite of 1% extreme precipitation days during June to September of 1979–2008 and changes for future 1% extreme precipitation days composite, respectively. There are 37 days with 1% extreme precipitation, i.e., the 1% largest daily precipitation averaged over SSTP during June to September in historical

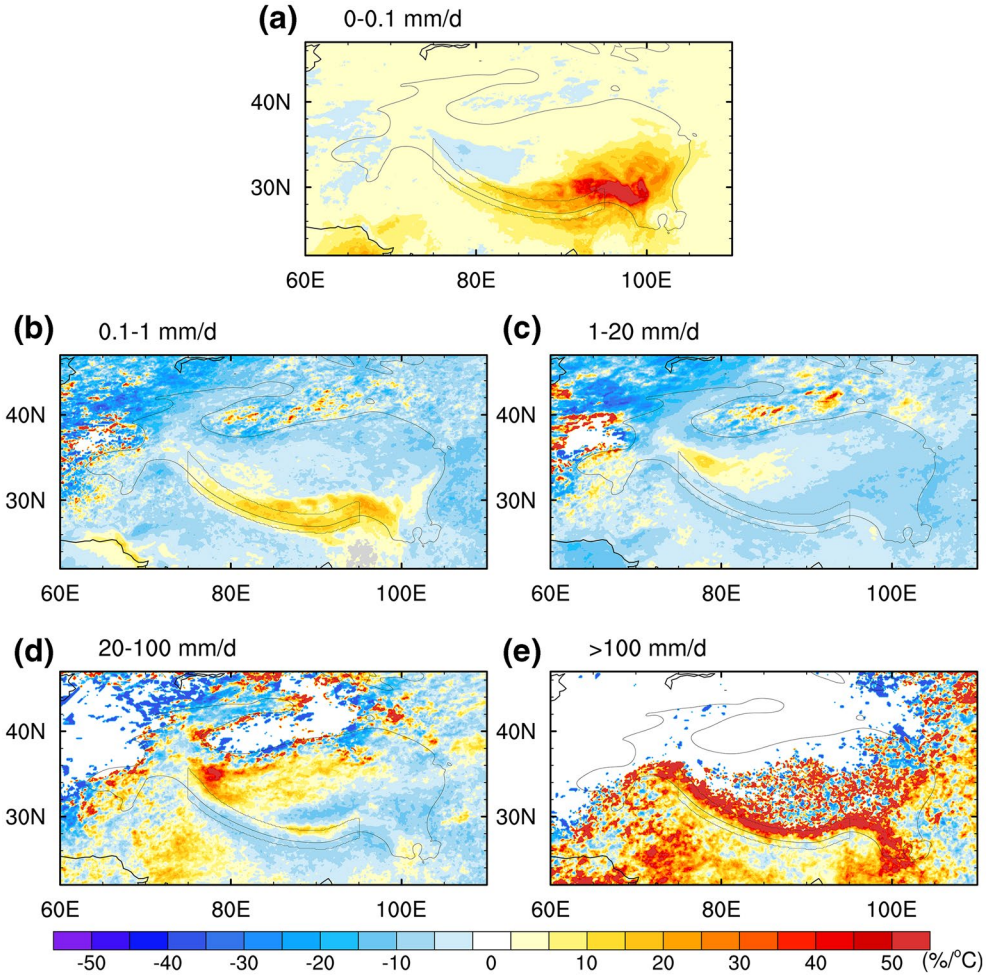

Figure 7. Spatial distributions of precipitation probability percentage changes (%/°C) for five precipitation ranges per degree global warming for June to September during future period 2075–2104 relative to historical period 1979–2008 from NICAM. The black lines show 2000-m contour line and SSTP area. NICAM, Nonhydrostatic ICosahedral Atmospheric Model; SSTP, southern slope of Tibetan Plateau.

or future period. Over most of the Tibetan Plateau and the south surrounding regions, NICAM presents the weak summer-mean upward flow (Figure 11a). For the composite of extreme precipitation days, strong westerlies flow into SSTP from the south, which are accompanied by stronger ascent velocities over SSTP, leading to the extreme precipitation (Figure 11b). NICAM projects easterly wind changes over the south of SSTP for future period (Figure 11c), which is generally opposite with historical period (Figure 11a). The circulation changes therefore may lead to the decrease of mean precipitation over the SSTP. The easterly wind changes also appear to the southeast of SSTP (Figure 11d), and they are generally opposite to the westerlies associated with extreme precipitation (Figure 11b). The maximum ascent velocities over southeast SSTP will decrease in the future which may lead to weaker extreme precipitation, but increasing ascent velocities appear to be over the central and western SSTP. The westward shift of the center of vertical velocity is in a good agreement with the increasing extreme precipitation over central SSTP (Figure 9b3).

Thermodynamic effect is also crucial for precipitation. Figure 12 shows the specific humidity (g/kg) vertically averaged in total column from NICAM historical simulation (a and b) and future changes (c and d). The specific humidity decreases from south of the Tibetan Plateau to north and the meridional gradient is strongest over SSTP. The distributions of extreme precipitation days (Figures 12b and 12d) do not show significant difference with summer mean (Figures 12a and 12c), implying that the extreme precipitation results mainly from dynamic effect for both the historical period and future changes, as shown in Fig-

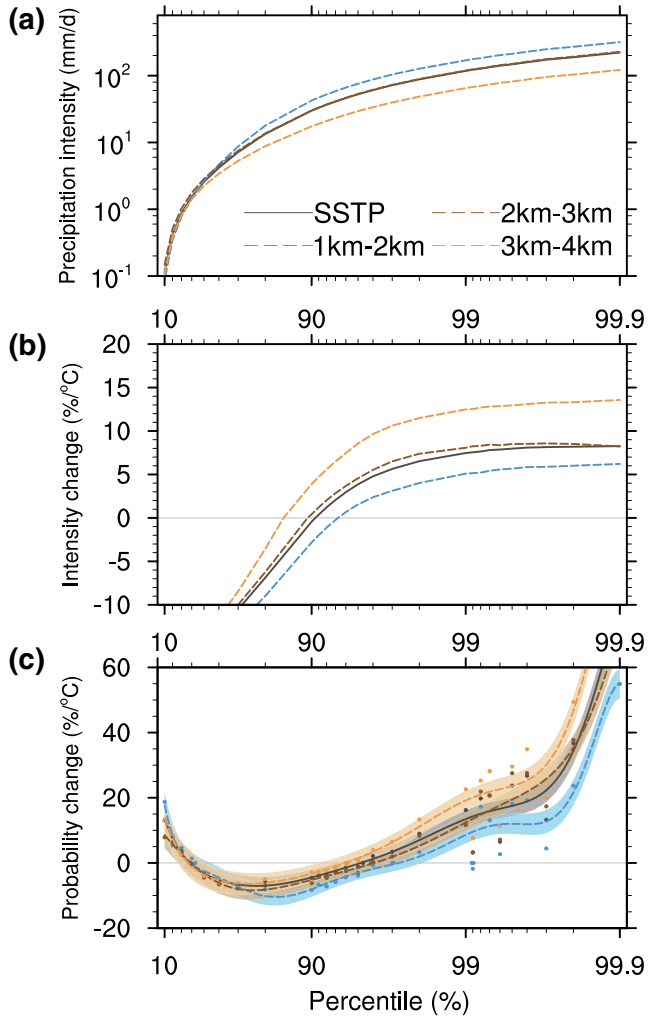

Figure 8. (a) Precipitation intensity (mm/d) corresponding to different percentiles (%) for June to September during historical period 1979–2008 averaged over SSTP and parts of SSTP from NICAM. Percentage change of (b) precipitation intensity and (c) precipitation probability (%/°C) corresponding to different percentiles for June to September during future period 2075–2104 relative to historical period per degree global warming. The dots in (c) are the changes for precipitation probability with an increment of 10%, 1%, 0.1%. The lines are polynomial fitting curves and the shades are 95% confidence boundaries. NICAM, Nonhydrostatic ICosahedral Atmospheric Model; SSTP, southern slope of Tibetan Plateau.

ure 11. On the other hand, the spatial patterns of future specific humidity changes are similar to the historical distributions, which suggests that the gradient will become larger in the future. The strengthening meridional specific humidity gradient under global warming suggests that there will be more water vapor transport over SSTP even without the strengthening circulation, which means the thermodynamic effect may be responsible for the future precipitation change rather than dynamic effect.

In summary, the westerly wind over the south of SSTP will generally become weaker and the meridional specific humidity gradient over SSTP will become stronger under global warming. For the mean precipitation over the SSTP, the dynamic and thermodynamic effects tend to cancel each other, leading to a small overall change. For the extreme precipitation, its increase over SSTP is caused by the thermodynamic effect. This result is consistent with previous studies (e.g., Pfahl et al., 2017), but gives a specific perspective over SSTP.

5. Conclusions and Discussions

The southern slope of Tibetan Plateau is one of the rainiest regions in the world where geological hazards caused by extreme precipitation result in serious damages. In this study, we first evaluate the daily precipitation simulation over the Tibetan Plateau from a 14 km mesh global nonhydrostatic model, NICAM, with the GPM satellite observation for June to September during 2001–2008. Then we examine the future projection of mean precipitation and extreme precipitation at the end of 21st century under global warming from NICAM and discuss the elevation dependent precipitation changes over SSTP.

Precipitation over the Tibetan Plateau decreases from the southeast to the northwest and exhibits precipitation extremes and zonal distribution along the topography over SSTP where precipitation concentrates on monsoon season (June to September). NICAM can reproduce the spatial pattern of precipitation over the Tibetan Plateau and the seasonal cycle as GPM observation. NICAM can also reproduce the topography features of rainfall over SSTP: the probability of heavy precipitation larger than 20 mm/d is much higher over SSTP than other regions and the probability decreases as elevation becomes higher. But NICAM overestimates precipitation over most Tibetan Plateau, which is a common bias of current climate models. Specifically, NICAM underestimates nonprecipitation probability but overestimates heavy precipitation probability.

Over the whole SSTP, total summer precipitation projected by NICAM change slightly under global warming. Future precipitation changes exhibit variations over SSTP depending on elevation. Mean precipitation will decrease 3.5% over low-level SSTP (1–2 km) but increase 2.6% and 9.2% over middle-level (2–3 km) and high-level SSTP (3–4 km). Nonprecipitation probability will increase while light precipitation probability will decrease in the future over SSTP. Heavy precipitation probability will increase more significantly, especially over higher level SSTP.

In comparison with total precipitation, the extreme precipitation probability and intensity over SSTP exhibit much more remarkable changes under global warming. Extreme precipitation intensity will increase ~8%/°C and extreme precipitation probability will increase up to ~50%/°C in the future. The increases of extreme precipitation probability and intensity over high-level SSTP are more obvious than over low-level SSTP. The extreme precipitation probability change over SSTP presents high consistency with topography distribution of Tibetan Plateau. In addition, SSTP is one of the regions in the north hemisphere showing the

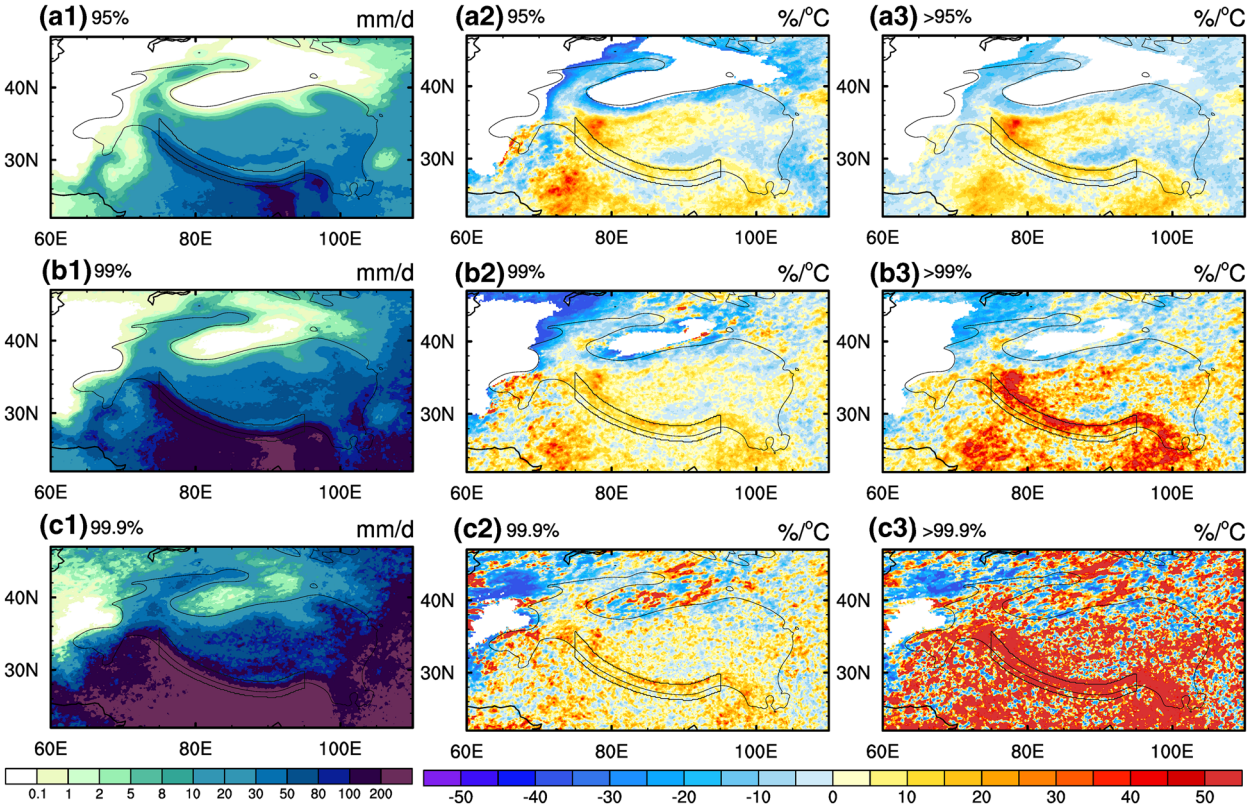

Figure 9. (a1–c1) Spatial distribution of precipitation intensity (mm/d) corresponding to 95%, 99%, 99.9% percentiles for June to September during historical period 1979–2008 from NICAM. Percentage changes (%/°C) of (a2–c2) precipitation intensity and (a3–c3) precipitation probability for June to September during future period 2075–2104 relative to historical period per degree global warming. The areas where precipitation intensity for historical period is <0.1 mm/d are shaded by white color. The black lines show 2000-m contour line and SSTP area. NICAM, Nonhydrostatic ICosahedral Atmospheric Model; SSTP, southern slope of Tibetan Plateau.

largest future extreme precipitation probability increase. In contrast to the weakening circulation changes over SSTP and surrounding region, the strengthened meridional specific humidity gradient is responsible for the extreme precipitation increasing.

The present study shows a decrease (increase) of total precipitation over low- (high-) level SSTP but an increase in extreme precipitation throughout the SSTP under global warming. The relationship between the changes in total and extreme precipitation and the physical mechanisms for these changes remain unknown. Why does the extreme precipitation increase even when the total precipitation decreases over low-level SSTP? How much of the changes in total precipitation can be attributed to extreme precipitation changes, given that they have opposite signs of changes? By considering more significant increase in extreme precipitation than the total precipitation over high-level SSTP, are there any other factors, in addition to total precipitation increase, contributing to the extreme precipitation increase over this region? Do a strong diurnal cycle of precipitation over the SSTP (Chen, 2020; Hirose & Kenji, 2005; Romatschke & Houze, 2011) and its changes play a role in affecting extreme precipitation change under global warming and the distinction between low-level and high-level SSTP? The final but important question might be: Are the SSTP precipitation changes dependent on model? This study uses only one model, and thus whether the robust extreme precipitation increase over SSTP is projected by other high-resolution models remains an open question.

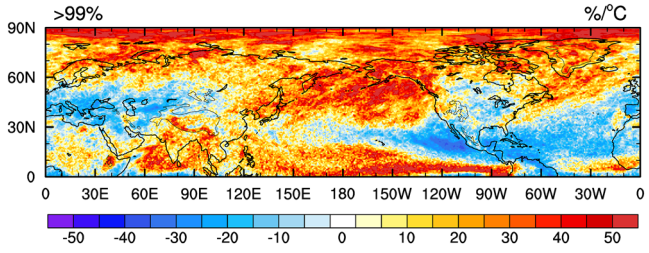

Figure 10. Spatial distribution of percentage change (%/°C) of probability for precipitation intensity larger than historical 99% percentile per degree global warming for June to September of future period 2075–2104 relative to historical period 1979–2008 over the Northern Hemisphere. The black lines show 2000-m contour line.

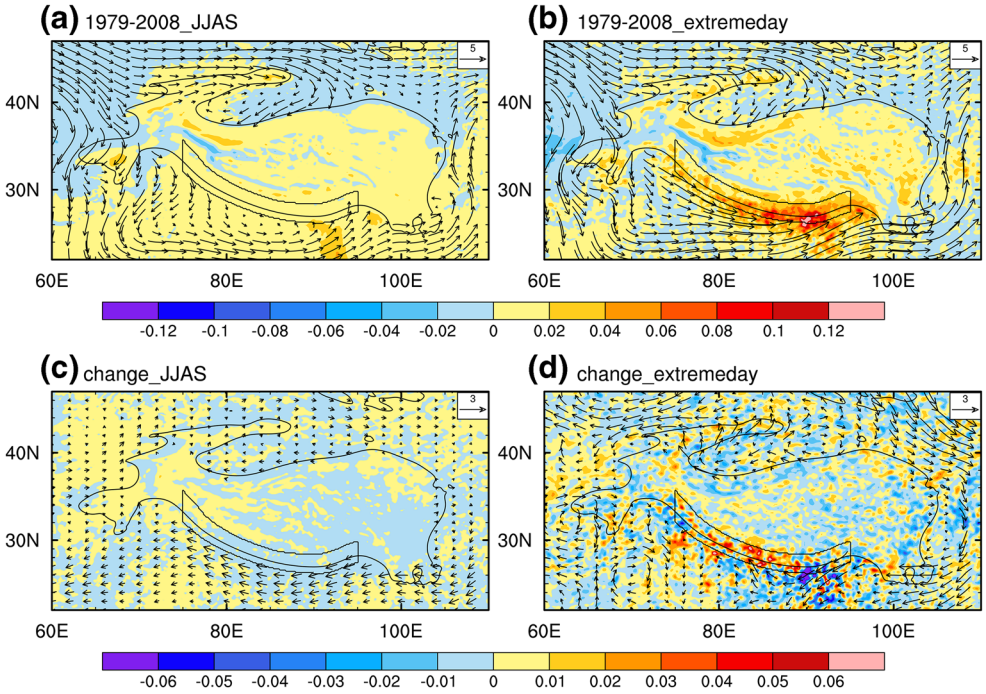

Figure 11. Spatial distributions of horizontal wind (m/s) at 700 hPa (vector) and vertical velocity (m/s) at 500 hPa (color) from NICAM simulation for the average of (a) all days during June to September of 1979–2008, (b) 1% extreme precipitation days (about 37 days in 30 years). (c and d) Same as (a and b), but for future changes for 2075–2104 relative to 1979–2008. Note that positive values represent upward motion. NICAM, Nonhydrostatic ICosahedral Atmospheric Model.

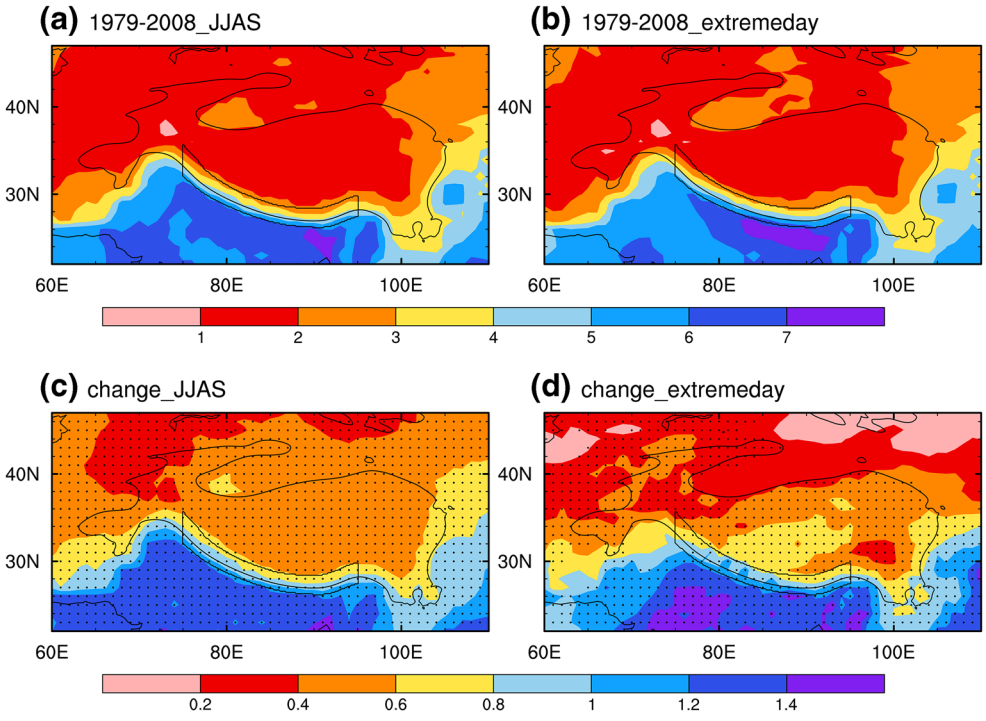

Figure 12. Same as Figure 11, but for specific humidity (g/kg) vertically averaged in total column. The dotted area indicates the change is statistically significant at the 95% confidence level (Student's *t*-test).

A better understanding of the precipitation characteristics over SSTP and their future changes can contribute to disaster-mitigation plans for this and downstream regions under global warming. The countries located in SSTP, e.g., Nepal and Bhutan, are facing a number of serious climate-fragility risks. Floods and landslides caused by extreme rainfall damage infrastructure, slow economic development, and cause hundreds to thousands of fatalities each year (Froude & Petley, 2018; Petley et al., 2007), which will be more serious in the warming future (Kirschbaum et al., 2020). Besides, the River Ganges, through some of Asia's most densely populated regions, originates in the Himalayas. The rainfall amount changes over SSTP can affect the river's flow and the surrounding hundreds of millions of people and wildlife. This work, based on the simulated results of one high-resolution climate model, suggests the necessity of further investigations on this specific region, which will be useful for decision making in South Asian countries.

Data Availability Statement

The terms and guideline of NICAM data can be accessed from http://nicam.jp/hiki/?Research+Collaborations. GPM data can be accessed from https://gpm1.gesdisc.eosdis.nasa.gov/data/GPM_L3/GPM_3IMERGDF.06/. NOAA ETOPO1 data are from https://ngdc.noaa.gov/mgg/global/global.html.

Acknowledgments
This study was supported by The Second Tibetan Plateau Scientific Expedition and Research (STEP) program (Grant 2019QZKK0102). Q. Fu was supported by the Office of Science (BER), U.S. Department of Energy, under Grant DE-SC0018190. C. Kodama was supported by Program for Promoting Researches on the Supercomputer Fugaku (Large Ensemble Atmospheric and Environmental Prediction for Disaster Prevention and Mitigation), which is promoted by the Ministry of Education, Culture, Sports, Science, and Technology (MEXT), Japan. All the NICAM runs were performed on the K computer at the RIKEN Advanced Institute for Computational Science (Proposal number hp120279, hp130010, and hp140219).

References

Ali, S., Li, D., Congbin, F., & Khan, F. (2015). Twenty first century climatic and hydrological changes over Upper Indus Basin of Himalayan region of Pakistan. *Environmental Research Letters*, *10*(1), 014007.

Anders, A. M., Roe, G. H., Hallet, B., Montgomery, D. R., Finnegan, N. J., & Putkonen, J. (2006). Spatial patterns of precipitation and topography in the Himalaya. *Special Papers-Geological Society of America*, *398*, 39. https://doi.org/10.1130/2006.2398(03)

Bao, Q., & Li, J. (2020). Progress in climate modeling of precipitation over the Tibetan Plateau. *National Science Review*, *7*(3), 486–487. https://doi.org/10.1093/nsr/nwaa006

Bhatt, B. C., & Nakamura, K. (2005). Characteristics of monsoon rainfall around the Himalayas revealed by TRMM precipitation radar. *Monthly Weather Review*, *133*(1), 149–165.

Bibi, S., Wang, L., Li, X., Zhou, J., Chen, D., & Yao, T. (2018). Climatic and associated cryospheric, biospheric, and hydrological changes on the Tibetan Plateau: A review. *International Journal of Climatology*, *38*, e1–e17. https://doi.org/10.1002/joc.5411

Bookhagen, B., & Burbank, D. W. (2006). Topography, relief, and TRMM-derived rainfall variations along the Himalaya. *Geophysical Research Letters*, *33*, L08405. https://doi.org/10.1029/2006gl026037

Bookhagen, B., & Burbank, D. W. (2010). Toward a complete Himalayan hydrological budget: Spatiotemporal distribution of snowmelt and rainfall and their impact on river discharge. *Journal of Geophysical Research*, *115*, F03019. https://doi.org/10.1029/2009JF001426

Chen, G. (2020). Diurnal cycle of the Asian summer monsoon: Air pump of the second kind. *Journal of Climate*, *33*(5), 1747–1775. https://doi.org/10.1175/jcli-d-19-0210.1

Chen, G., Norris, J., Neelin, J. D., Lu, J., Leung, L. R., & Sakaguchi, K. (2019). Thermodynamic and dynamic mechanisms for hydrological cycle intensification over the full probability distribution of precipitation events. *Journal of the Atmospheric Sciences*, *76*(2), 497–516.

Chen, L., & Frauenfeld, O. W. (2014). A comprehensive evaluation of precipitation simulations over China based on CMIP5 multimodel ensemble projections. *Journal of Geophysical Research: Atmospheres*, *119*, 5767–5786. https://doi.org/10.1002/2013JD021190

Collier, E., & Immerzeel, W. W. (2015). High-resolution modeling of atmospheric dynamics in the Nepalese Himalaya. *Journal of Geophysical Research: Atmospheres*, *120*, 9882–9896. https://doi.org/10.1002/2015jd023266

Dai, A., Zhao, T., & Chen, J. (2018). Climate change and drought: A precipitation and evaporation perspective. *Current Climate Change Reports*, *4*(3), 301–312. https://doi.org/10.1007/s40641-018-0101-6

Dirmeyer, P. A., Cash, B. A., Kinter, J. L., Jung, T., Marx, L., Satoh, M., et al. (2011). Simulating the diurnal cycle of rainfall in global climate models: Resolution versus parameterization. *Climate Dynamics*, *39*(1–2), 399–418. https://doi.org/10.1007/s00382-011-1127-9

Dong, W., Lin, Y., Wright, J. S., Ming, Y., Xie, Y., Wang, B., et al. (2016). Summer rainfall over the southwestern Tibetan Plateau controlled by deep convection over the Indian subcontinent. *Nature Communications*, *7*, 10925. https://doi.org/10.1038/ncomms10925

Duan, A., & Wu, G. (2005). Role of the Tibetan Plateau thermal forcing in the summer climate patterns over subtropical Asia. *Climate Dynamics*, *24*(7–8), 793–807.

Fischer, E. M., & Knutti, R. (2015). Anthropogenic contribution to global occurrence of heavy-precipitation and high-temperature extremes. *Nature Climate Change*, *5*(6), 560–564.

Fischer, E. M., & Knutti, R. (2016). Observed heavy precipitation increase confirms theory and early models. *Nature Climate Change*, *6*(11), 986–991. https://doi.org/10.1038/nclimate3110

Froude, M. J., & Petley, D. (2018). Global fatal landslide occurrence from 2004 to 2016. *Natural Hazards and Earth System Sciences*, *18*, 2161–2181.

Fu, Y., Pan, X., Xian, T., Liu, G., Zhong, L., Liu, Q., et al. (2017). Precipitation characteristics over the steep slope of the Himalayas in rainy season observed by TRMM PR and VIRS. *Climate Dynamics*, *51*(5–6), 1971–1989. https://doi.org/10.1007/s00382-017-3992-3

Gao, G., Chen, Q., Cai, H., Li, Y., & Wang, Z. (2019). Comprehensive characteristics of summer deep convection over Tibetan Plateau and its south slope from the Global Precipitation Measurement Core Observatory. *Atmosphere*, *10*(1), 9. https://doi.org/10.3390/atmos10010009

Gao, J., Masson-Delmotte, V., Yao, T., Tian, L., Risi, C., & Hoffmann, G. (2011). Precipitation water stable isotopes in the south Tibetan Plateau: Observations and modeling. *Journal of Climate*, *24*(13), 3161–3178.

Giorgi, F., Torma, C., Coppola, E., Ban, N., Schär, C., & Somot, S. (2016). Enhanced summer convective rainfall at Alpine high elevations in response to climate warming. *Nature Geoscience*, *9*(8), 584–589. https://doi.org/10.1038/ngeo2761

Hansen, J., & Sato, M. (2004). Greenhouse gas growth rates. *Proceedings of the National Academy of Sciences of the United States of America*, *101*(46), 16109–16114.
Hirose, M., & Kenji, N. (2005). Spatial and diurnal variation of precipitation systems over Asia observed by the TRMM precipitation radar. *Journal of Geophysical Research*, *110*, D05106. https://doi.org/10.1029/2004jd004815
Hou, A. Y., Kakar, R. K., Neeck, S., Azarbarzin, A. A., Kummerow, C. D., Kojima, M., et al. (2014). The global precipitation measurement mission. *Bulletin of the American Meteorological Society*, *95*(5), 701–722.
Huffman, G. J., Bolvin, D. T., Braithwaite, D., Hsu, K., Joyce, R., Xie, P., & Yoo, S.-H. (2015). NASA global precipitation measurement (GPM) integrated multi-satellite retrievals for GPM (IMERG). *Algorithm Theoretical Basis Document (ATBD) Version*, *4*, 26.
Kajikawa, Y., Miyamoto, Y., Yoshida, R., Yamaura, T., Yashiro, H., & Tomita, H. (2016). Resolution dependence of deep convections in a global simulation from over 10-kilometer to sub-kilometer grid spacing. *Progress in Earth and Planetary Science*, *3*(1), 16.
Karki, R., Su, H., Gerlitz, L., Schickhoff, U., Scholten, T., & Böhner, J. (2017). Quantifying the added value of convection-permitting climate simulations in complex terrain: A systematic evaluation of WRF over the Himalayas. *Earth System Dynamics*, *8*(3), 507–528. https://doi.org/10.5194/esd-8-507-2017
Kharin, V. V., Zwiers, F. W., Zhang, X., & Wehner, M. (2013). Changes in temperature and precipitation extremes in the CMIP5 ensemble. *Climatic Change*, *119*(2), 345–357. https://doi.org/10.1007/s10584-013-0705-8
Kirschbaum, D., Kapnick, S., Stanley, T., & Pascale, S. (2020). Changes in extreme precipitation and landslides over High Mountain Asia. *Geophysical Research Letters*, *47*, e2019GL085347. https://doi.org/10.1029/2019GL085347
Kodama, C., Yamada, Y., Noda, A. T., Kikuchi, K., Kajikawa, Y., Nasuno, T., et al. (2015). A 20-year climatology of a NICAM AMIP-type simulation. *Journal of the Meteorological Society of Japan Series II*, *93*(4), 393–424. https://doi.org/10.2151/jmsj.2015-024
Kuang, X. X., & Jiao, J. J. (2016). Review on climate change on the Tibetan Plateau during the last half century. *Journal of Geophysical Research: Atmospheres*, *121*, 3979–4007. https://doi.org/10.1002/2015jd024728
Lei, Y. B., Yang, K., Wang, B., Sheng, Y. W., Bird, B. W., Zhang, G. Q., & Tian, L. D. (2014). Response of inland lake dynamics over the Tibetan Plateau to climate change. *Climatic Change*, *125*(2), 281–290. https://doi.org/10.1007/s10584-014-1175-3
Leung, L. R., & Qian, Y. (2003). The sensitivity of precipitation and snowpack simulations to model resolution via nesting in regions of complex terrain. *Journal of Hydrometeorology*, *4*(6), 1025–1043.
Li, P., Furtado, K., Zhou, T., Chen, H., & Li, J. (2020). Convection-permitting modelling improves simulated precipitation over the central and eastern Tibetan Plateau. *Quarterly Journal of the Royal Meteorological Society*, 1–22. https://doi.org/10.1002/qj.3921
Lin, C., Chen, D., Yang, K., & Ou, T. (2018). Impact of model resolution on simulating the water vapor transport through the central Himalayas: Implication for models' wet bias over the Tibetan Plateau. *Climate Dynamics*, *51*(9–10), 3195–3207. https://doi.org/10.1007/s00382-018-4074-x
Lin, L., Gettelman, A., Xu, Y., Wu, C., Wang, Z., Rosenbloom, N., et al. (2019). CAM6 simulation of mean and extreme precipitation over Asia: Sensitivity to upgraded physical parameterizations and higher horizontal resolution. *Geoscientific Model Development*, *12*(8), 3773–3793. https://doi.org/10.5194/gmd-12-3773-2019
Liu, X., Bai, A., & Liu, C. (2009a). Diurnal variations of summertime precipitation over the Tibetan Plateau in relation to orographically-induced regional circulations. *Environmental Research Letters*, *4*(4), 045203. https://doi.org/10.1088/1748-9326/4/4/045203
Liu, X., & Chen, B. (2000). Climatic warming in the Tibetan Plateau during recent decades. *International Journal of Climatology: A Journal of the Royal Meteorological Society*, *20*(14), 1729–1742.
Liu, X., Cheng, Z., Yan, L., & Yin, Z.-Y. (2009b). Elevation dependency of recent and future minimum surface air temperature trends in the Tibetan Plateau and its surroundings. *Global and Planetary Change*, *68*(3), 164.
Liu, X., & Dong, B. (2013). Influence of the Tibetan Plateau uplift on the Asian monsoon-arid environment evolution. *Chinese Science Bulletin*, *58*(34), 4277–4291. https://doi.org/10.1007/s11434-013-5987-8
Lu, D., & Yong, B. (2018). Evaluation and hydrological utility of the latest GPM IMERG V5 and GSMaP V7 precipitation products over the Tibetan Plateau. *Remote Sensing*, *10*(12), 2022. https://doi.org/10.3390/rs10122022
Mahoney, K., Alexander, M., Scott, J. D., & Barsugli, J. (2013). High-resolution downscaled simulations of warm-season extreme precipitation events in the Colorado front range under past and future climates. *Journal of Climate*, *26*(21), 8671–8689. https://doi.org/10.1175/jcli-d-12-00744.1
Mehran, A., AghaKouchak, A., & Phillips, T. J. (2014). Evaluation of CMIP5 continental precipitation simulations relative to satellite-based gauge-adjusted observations. *Journal of Geophysical Research: Atmospheres*, *119*, 1695–1707. https://doi.org/10.1002/2013JD021152
Miyamoto, Y., Kajikawa, Y., Yoshida, R., Yamaura, T., Yashiro, H., & Tomita, H. (2013). Deep moist atmospheric convection in a subkilometer global simulation. *Geophysical Research Letters*, *40*, 4922–4926. https://doi.org/10.1002/grl.50944
Mizuta, R., Adachi, Y., Yukimoto, S., & Kusunoki, S. (2008). Estimation of the future distribution of sea surface temperature and sea ice using the CMIP3 multi-model ensemble mean CMIP3. *Technical Reports of the Meteorological Research Institute*, *56*, 1–28.
Mueller, B., & Seneviratne, S. I. (2014). Systematic land climate and evapotranspiration biases in CMIP5 simulations. *Geophysical Research Letters*, *41*, 128–134. https://doi.org/10.1002/2013GL058055
Na, Y., Fu, Q., & Kodama, C. (2020). Precipitation probability and its future changes from a Global Cloud-Resolving Model and CMIP6 simulations. *Journal of Geophysical Research: Atmospheres*, *125*, e2019JD031926. https://doi.org/10.1029/2019JD031926
Palazzi, E., von Hardenberg, J., Terzago, S., & Provenzale, A. (2015). Precipitation in the Karakoram-Himalaya: A CMIP5 view. *Climate Dynamics*, *45*(1–2), 21–45. https://doi.org/10.1007/s00382-014-2341-z
Panday, P. K., Thibeault, J., & Frey, K. E. (2015). Changing temperature and precipitation extremes in the Hindu Kush-Himalayan region: An analysis of CMIP3 and CMIP5 simulations and projections. *International Journal of Climatology*, *35*(10), 3058–3077.
Petley, D. N., Hearn, G. J., Hart, A., Rosser, N. J., Dunning, S. A., Oven, K., & Mitchell, W. A. (2007). Trends in landslide occurrence in Nepal. *Natural Hazards*, *43*(1), 23–44.
Pfahl, S., O'Gorman, P. A., & Fischer, E. M. (2017). Understanding the regional pattern of projected future changes in extreme precipitation. *Nature Climate Change*, *7*(6), 423–427.
Romatschke, U., & Houze, R. A. (2011). Characteristics of precipitating convective systems in the South Asian Monsoon. *Journal of Hydrometeorology*, *12*(1), 3–26. https://doi.org/10.1175/2010jhm1289.1
Salerno, F., Guyennon, N., Thakuri, S., Viviano, G., Romano, E., Vuillermoz, E., et al. (2015). Weak precipitation, warm winters and springs impact glaciers of south slopes of Mt. Everest (central Himalaya) in the last 2 decades (1994–2013). *The Cryosphere*, *9*(3), 1229–1247. https://doi.org/10.5194/tc-9-1229-2015
Sato, T., Miura, H., & Satoh, M. (2007). Spring diurnal cycle of clouds over Tibetan Plateau: Global cloud-resolving simulations and satellite observations. *Geophysical Research Letters*, *34*, L18816. https://doi.org/10.1029/2007gl030782

Sato, T., Yoshikane, T., Satoh, M., Miura, H., & Fujinami, H. (2008). Resolution dependency of the diurnal cycle of convective clouds over the Tibetan Plateau in a mesoscale model. *Journal of the Meteorological Society of Japan Series II*, *86*, 17–31.

Satoh, M., Matsuno, T., Tomita, H., Miura, H., Nasuno, T., & Iga, S. (2008). Nonhydrostatic Icosahedral Atmospheric Model (NICAM) for global cloud resolving simulations. *Journal of Computational Physics*, *227*(7), 3486–3514. https://doi.org/10.1016/j.jcp.2007.02.006

Satoh, M., Tomita, H., Yashiro, H., Miura, H., Kodama, C., Seiki, T., et al. (2014). The Non-hydrostatic Icosahedral Atmospheric Model: Description and development. *Progress in Earth and Planetary Science*, *1*(1), 18. https://doi.org/10.1186/s40645-014-0018-1

Satoh, M., Yamada, Y., Sugi, M., Kodama, C., & Noda, A. T. (2015). Constraint on future change in global frequency of tropical cyclones due to global warming. *Journal of the Meteorological Society of Japan Ser II*, *93*(4), 489–500.

Shrestha, D., Singh, P., & Nakamura, K. (2012). Spatiotemporal variation of rainfall over the central Himalayan region revealed by TRMM precipitation radar. *Journal of Geophysical Research*, *117*, D22106. https://doi.org/10.1029/2012jd018140

Skofronick-Jackson, G., Petersen, W. A., Berg, W., Kidd, C., Stocker, E. F., Kirschbaum, D. B., et al. (2017). The Global Precipitation Measurement (GPM) mission for science and society. *Bulletin of the American Meteorological Society*, *98*(8), 1679–1695.

Su, F., Duan, X., Chen, D., Hao, Z., & Cuo, L. (2013). Evaluation of the global climate models in the CMIP5 over the Tibetan Plateau. *Journal of Climate*, *26*(10), 3187–3208. https://doi.org/10.1175/jcli-d-12-00321.1

Su, F., Zhang, L., Ou, T., Chen, D., Yao, T., Tong, K., & Qi, Y. (2016). Hydrological response to future climate changes for the major upstream river basins in the Tibetan Plateau. *Global and Planetary Change*, *136*, 82–95.

Takahashi, H. G., Kamizawa, N., Nasuno, T., Yamada, Y., Kodama, C., Sugimoto, S., & Satoh, M. (2020). Response of the Asian summer monsoon precipitation to global warming in a high-resolution global nonhydrostatic model. *Journal of Climate*, *33*(18), 8147–8164.

Tian, Y., & Peters-Lidard, C. D. (2010). A global map of uncertainties in satellite-based precipitation measurements. *Geophysical Research Letters*, *37*, L24407. https://doi.org/10.1029/2010GL046008

Tomita, H. (2008). New microphysical schemes with five and six categories by diagnostic generation of cloud ice. *Journal of the Meteorological Society of Japan Ser II*, *86*, 121–142.

Tomita, H., & Satoh, M. (2004). A new dynamical framework of nonhydrostatic global model using the icosahedral grid. *Fluid Dynamics Research*, *34*(6), 357.

Torma, C., Giorgi, F., & Coppola, E. (2015). Added value of regional climate modeling over areas characterized by complex terrain-Precipitation over the Alps. *Journal of Geophysical Research: Atmospheres*, *120*, 3957–3972. https://doi.org/10.1002/2014jd022781

Wu, G., Liu, Y., Zhang, Q., Duan, A., Wang, T., Wan, R., et al. (2007). The influence of mechanical and thermal forcing by the Tibetan Plateau on Asian climate. *Journal of Hydrometeorology*, *8*(4), 770–789.

Wu, G., & Zhang, Y. (1998). Tibetan Plateau forcing and the timing of the monsoon onset over South Asia and the South China Sea. *Monthly Weather Review*, *126*(4), 913–927. https://doi.org/10.1175/1520-0493(1998)126<0913:tpfatt>2.0.co;2

Wu, J., Xu, Y., & Gao, X.-J. (2017). Projected changes in mean and extreme climates over Hindu Kush Himalayan region by 21 CMIP5 models. *Advances in Climate Change Research*, *8*(3), 176–184.

Xu, J., Yang, D., Yi, Y., Lei, Z., Chen, J., & Yang, W. (2008). Spatial and temporal variation of runoff in the Yangtze River basin during the past 40 years. *Quaternary International*, *186*(1), 32–42.

Yang, K., Guyennon, N., Ouyang, L., Tian, L., Tartari, G., & Salerno, F. (2018). Impact of summer monsoon on the elevation-dependence of meteorological variables in the south of central Himalaya. *International Journal of Climatology*, *38*(4), 1748–1759. https://doi.org/10.1002/joc.5293

Yang, T., Hao, X., Shao, Q., Xu, C.-Y., Zhao, C., Chen, X., & Wang, W. (2012). Multi-model ensemble projections in temperature and precipitation extremes of the Tibetan Plateau in the 21st century. *Global and Planetary Change*, *80–81*, 1–13. https://doi.org/10.1016/j.gloplacha.2011.08.006

Yao, T., Thompson, L., Yang, W., Yu, W., Gao, Y., Guo, X., et al. (2012). Different glacier status with atmospheric circulations in Tibetan Plateau and surroundings. *Nature Climate Change*, *2*(9), 663–667. https://doi.org/10.1038/nclimate1580

Yu, R., Li, J., Zhang, Y., & Chen, H. (2015). Improvement of rainfall simulation on the steep edge of the Tibetan Plateau by using a finite-difference transport scheme in CAM5. *Climate Dynamics*, *45*(9–10), 2937–2948. https://doi.org/10.1007/s00382-015-2515-3

Zhang, A., Fu, Y., Chen, Y., Liu, G., & Zhang, X. (2018a). Impact of the surface wind flow on precipitation characteristics over the southern Himalayas: GPM observations. *Atmospheric Research*, *202*, 10–22. https://doi.org/10.1016/j.atmosres.2017.11.001

Zhang, H., Gao, Y., Xu, J., Xu, Y., & Jiang, Y. (2019). Decomposition of future moisture flux changes over the Tibetan Plateau projected by global and regional climate models. *Journal of Climate*, *32*(20), 7037–7053. https://doi.org/10.1175/jcli-d-19-0200.1

Zhang, R., Jiang, D., Zhang, Z., & Yu, E. (2015). The impact of regional uplift of the Tibetan Plateau on the Asian monsoon climate. *Palaeogeography, Palaeoclimatology, Palaeoecology*, *417*, 137–150.

Zhang, S., Wang, D., Qin, Z., Zheng, Y., & Guo, J. (2018b). Assessment of the GPM and TRMM precipitation products using the rain gauge network over the Tibetan Plateau. *Journal of Meteorological Research*, *32*(2), 324–336. https://doi.org/10.1007/s13351-018-7067-0

Zhu, Y. Y., & Yang, S. (2020). Evaluation of CMIP6 for historical temperature and precipitation over the Tibetan Plateau and its comparison with CMIP5. *Advances in Climate Change Research*. https://doi.org/10.1016/j.accre.2020.08.001